Chapter 8
Polyhedral Oligomeric Silsesquioxanes in Space Applications

Henry W. Brandhorst, Jr.

8.1   The Space Environment

The space environment around the earth is exceptionally complex and has a significant impact on the lifetime and performance of any orbiting satellite. At least six factors influence the satellite: atomic oxygen (AO), electrons and protons trapped in the earth's magnetic field, solar flare protons, solar radiation, thermal cycling resulting from the passage of the spacecraft through the Earth's shadow, and debris. To deal with all these environmental factors, a space power system that uses solar cells is built to ameliorate these problems. First the solar cells are covered with a protective glass cover that contains a cerium additive. This absorbs ultraviolet light that would damage the silicone rubber adhesive that attaches the cover to the cell. The primary purpose of this cover is to limit the radiation damage from electrons and protons. The cells are usually then attached to a rigid composite substrate that can be oriented to track the sun as the satellite moves around the earth. The cover glass process is expensive, and there has long been a desire to find a material that would be resistant to these space environmental factors. POS additives have particular attributes that make them especially attractive for use in photovoltaic space power systems.

Atomic oxygen is the first hazard that a solar array must overcome. Atomic oxygen is created in earth orbit by the interaction of sunlight with residual oxygen molecules at the top of the atmosphere. Ultraviolet light transforms the oxygen molecule into a single oxygen atom, hence the term "atomic oxygen". It is the most prevalent atmospheric species in Low Earth Orbit (LEO), at about 300 km altitude. These atoms are highly reactive and are in high concentrations, therefore at a

Henry W. Brandhorst, Jr.
Director, Space Research Institute
Auburn University, AL 36849-5320

satellite velocity of about 17,000 miles per hour (7.6 km s^{-1}), spacecraft materials are eaten away rapidly [1,2,3,4]. The actual atomic oxygen flux on a spacecraft varies with altitude, but the flux ranges from ~10^{12} – 10^{14} atoms cm^{-2} s^{-1}. The collision energy is about 5 eV, while the energy of a C-C bond is only ~4 eV. Therefore, polymeric materials such as Kapton® and polymer-matrix carbon-fiber composites are especially eroded by atomic oxygen, and this impacts spacecraft performance and/or structural failure. Kapton® is used as a substrate for solar arrays as well as part of thermal control blankets, so the problem of erosion can be severe. Thus, any solar array has to be designed to withstand attack by atomic oxygen. In general, the approach used to develop either protective coatings for polymers, or inherently durable polymers, has focused upon the use of metal atoms that, upon exposure to atomic oxygen, form stable non-volatile oxides that resist further attack. For example, silicones have been incorporated into polyimides, where exposure to atomic oxygen will cause the formation of sufficient silicon dioxide at the surface to protect the underlying polymers. For example, a polydimethylsiloxane-polyimide mixture has been developed [5]. However, the spatial variation and low surface concentration of the silicone constituents allowed gradual atomic oxygen attack of the bulk material when evaluated in ground laboratory testing.

Polydimethylsiloxanes, which contain one silicon atom per oxygen atom, are gradually converted to silica by atomic oxygen attack. In this process the loss of the methyl groups and conversion to SiO$_2$ results in the shrinkage of the polymer, with attendant cracks that can lead to attack of any underlying polymers [6,7]. However, the use of textured surfaces on the polydimethylsiloxanes has produced coatings that do not crack from the same atomic oxygen fluences that would cause the smooth surfaces on the same materials to crack [8]. Silsesquioxanes have shown promise over conventional polydimethylsiloxanes in that they contain 1.5 silicon atoms per oxygen atom, and do not show the shrinkage and cracking phenomena associated with polydimethylsiloxanes. These materials will be discussed later.

The Earth is encircled by electrons and protons trapped in the Earth's magnetic field. These radiation belts were discovered in 1958 by Dr. James Van Allen and carry his name. They are located in two primary regions above the Earth and along the Earth's magnetic plane as shown in Fig. 8.1. The inner radiation belt consists primarily of high concentrations of energetic protons (>100 MeV) and some energetic electrons (~100 keV). It extends from about 100 to 10,000 km (0.016 to 1.6 Earth radii) above the Earth's surface. The outer radiation belt consists primarily of high energy electrons, and extends from about 19,000 to 64,000 km (3 to 10 Earth radii) above the surface. This belt peaks at about 25,000 to 32,000 km (4-5 Earth radii). This belt contains electrons with energies from about 0.1 to 10 MeV. These energetic particles damage electronic devices such as solar cells by creating surface defects, and thus reducing output power. Thus protective cover glasses are used to limit the damage. The thicker the cover glass, the less will be the damage. However, any substitute material will also have to be resistant to these trapped electrons and protons. In addition, the amount of radiation a spacecraft receives depends upon its orbit. Satellites in LEO (<400 km) generally receive low doses of damaging radiation. Those satellites in geostationary space orbit (GEO) receive substantially
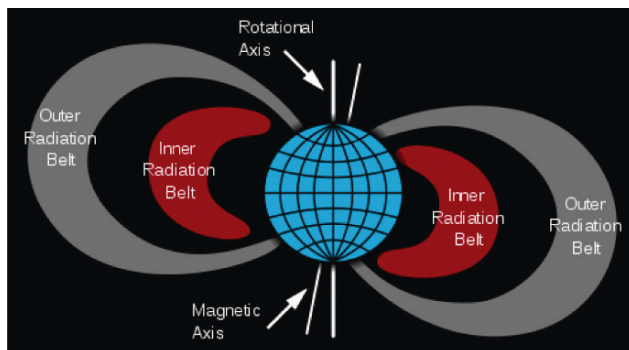
Fig. 8.1 Schematic drawing of the Earth's Van Allen radiation belts.

more, and those satellites in highly inclined orbits, or in mid-Earth orbits, receive the most radiation damage. In addition, the type of material in the solar cell also dictates the degree of damage.
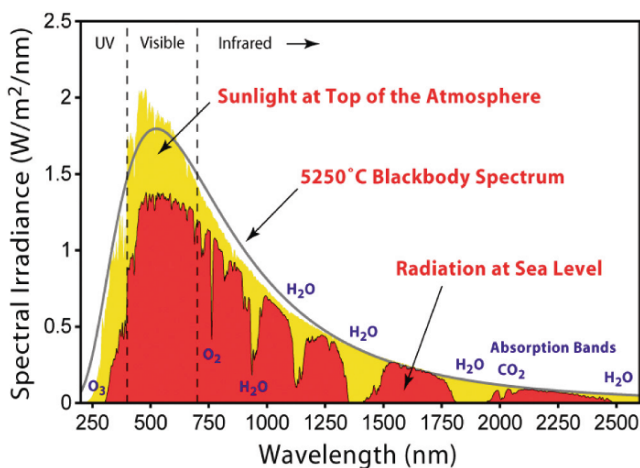
Fig. 8.2 Spectrum of solar radiation at the Earth

The next hazard for space vehicles traveling in Earth orbit is sunlight itself. The solar spectrum in space differs greatly from that of the sunlight that arrives at the Earth's surface. The sunlight that arrives at the top of the atmosphere is modified through absorption and scattering by atmospheric constituents such as water vapor, carbon dioxide, ozone, oxygen, nitrogen, dust and clouds. For a surface at sea level, the solar intensity reaching that surface is about 1,000 W m^{-2} when the sun is directly overhead. This represents a ~25% reduction in the sunlight intensity at the top of the atmosphere (~1360 W m^{-2}). The atmospheric absorption occurs in bands in the infrared region of the spectrum but almost uniformly across the visible and ultraviolet region of the spectrum, as shown in Fig. 8.2. The red curve shows the spectrum at the earth's surface while the yellow shows the outer space spectrum. In

space, the major parts of the spectrum that affect the lifetime of a satellite are the ultraviolet and vacuum ultraviolet regions, from 150 to 300 nm. This high energy light breaks chemical bonds and thus leads to the darkening of the adhesives used to attach the cover glasses to the solar cells. Thus efforts were directed toward finding a polyhedral oligomeric silsesquioxanes (POS)-based replacement for the traditional cover glasses.

8.2   Resistance of Siloxane Copolymers to Atomic Oxygen in Low Earth Orbit

As noted in the initial paper on POS materials in space [9], materials with resistance to degradation by the harsh conditions (e.g., atomic oxygen and UV light) present in LEO are essential for extended use of lightweight, polymeric structures in space [10,11]. As noted above, the degradation of carbon-based materials in the LEO environment is due to the presence of ground-state atomic oxygen that has been created from the photo-dissociation of molecular oxygen [12] combined with solar UV radiation, and with the 8 km s^{-1} orbital velocity of vehicles in LEO [13]. A class of non-carbon-based materials with rates of erosion one to two orders of magnitude slower than organic polymers in LEO has been developed. These are the siloxane polymers which, when exposed to atomic oxygen (AO), convert to a protective silica-like coating. In an attempt to utilize this desirable property, the seminal work in this field was performed using polyimide-siloxane (PISX) copolymers and polyhedral oligomeric silsequioxane (POS)-siloxane copolymers as coatings and matrix materials. The copolymers were used as the resin for PISX-carbon fiber composites. These composites were then exposed in LEO for 50 hours as part of the "Effect of Oxygen Interactions with Materials" (EOIM-III) experiment aboard the STS-46 NASA space shuttle flight [14].

     A composite made with a 37% loading of PISX with Celion 6000 carbon fibers had a density of 1.54 g cm^{-3}, a flexural strength of 194 Ksi, and a short beam shear strength of 8 Ksi. These properties were comparable to typical PMR-l5/graphite composites (having flexural strengths of ~235 Ksi), and hence were expected to be useful in similar applications. PMR-15 is a high temperature polyimide resin usually used with carbon fibers for excellent high temperature behavior, and Celion 6000 carbon fibers are commonly used in such composites. The fabrication conditions were chosen to demonstrate the feasibility of using PISX as the matrix for composites that would be suitable for space applications. The samples were flown on STS-46 in March 1992, and were exposed to the LEO environment in trays heated to 60 and 120 °C. The heated trays allowed investigation of the effect of temperature, atomic oxygen, and UV radiation on the composite samples. The samples were exposed to LEO for ~50 hours, the total A0 fluence was 2.2 x 10^{20} atom cm^{-2}, and the total time of exposure to the solar UV was 7.6 hours [9]. The investigation of the surface of

this PISX composite using X-ray photoelectron spectroscopy (XPS) reveaed that the siloxane-rich composite surface was oxidized to the silica-like material as expected. The following conclusions may be drawn from the experiments above: (1**)** PISX is a suitable matrix for composites for space applications; (2) PISX composites are *one-to-two orders of magnitude more resistant* to the simulated LEO environment than are standard polyimide composites; (3) PISX composites *erode more slowly* when far-UV radiation is combined with the atomic oxygen, in contrast to other materials, where UV radiation accelerates the degradation process.

In another corollary experiment, a POS-siloxane copolymer was developed to use as an LEO-resistant coating. These polyhedral oligomeric silsesquioxanes ($RSiO_{1.5}$) contain a silicon-oxygen ratio that is intermediate between that found in silica (SiO_2) and that found in siloxanes ($-R_2SiO-$). The composition is very similar to that found on the surface of silicon-based materials after exposure to atomic oxygen in LEO. A family of tractable POS-siloxane copolymers was fabricated. Evaluation of the resistance of this POS-siloxane copolymer to a simulated LEO environment was conducted. The samples were exposed to atomic oxygen with and without far-UV radiation. XPS analysis revealed that the surface of the copolymer samples became more silicon- and oxygen-rich after exposure to atomic oxygen, both with and without far-UV radiation.

Comparison of these results showed that the POS-siloxane copolymer had a greater resistance to the simulated LEO environment than PISX. The POS-siloxane copolymer actually gained weight during the exposures. Combining far-UV radiation with atomic oxygen does not significantly change the results. The samples were exposed to a simulated atomic oxygen fluence of 4.3×10^{21} atoms cm^{-3} both with and without UV exposure at 15 mW cm^{-2} (about 7 Earth suns equivalent). The samples gained weight, and the initial microcracks on the surface were actually healed by the atomic oxygen exposure. This annealing phenomenon seen for the POS-siloxane copolymers may result from surface heating, both from the heat of reaction (ΔH), and from absorption of the kinetic energy **(**2-3 eV) of the atomic oxygen. This also could be a significant advantage for these materials, since micro-cracking exposes a coated surface to the LEO environment and to accelerated degradation, and contributes to loss of long-term durability for composites used in space. This finding led to a more detailed study of the POS composites and their use in space.

Several series of ground tests were run on a range of POS compositions [15] with a hyperthermal atomic oxygen source [16]. This source is ultrahigh vacuum (UHV)-compatible, operates at room temperature, and produces a high-purity, hyperthermal, AO flux with an AO:OC ratio of $\sim 10^8$. These sources are superior to plasma sources because they operate at UHV pressures ($\sim 1.33 \times 10^7$ Pa) and produce hyperthermal, ground-state O atoms and negligible quantities of other species (e.g., ions, contaminants and UV radiation). The AO produced by this source has an energy of 2-5 eV (although the energy distribution within this range was not measured). A POS-polyurethane (PU) copolymer was produced by solvent casting from THF solutions of 5 mg cm^{-3} of each polymer. They were dried, cleaned and put

into the UHV chamber above.

XPS probes the near-surface region of a sample and yields a weighted average composition, with the atomic layers near the surface being weighted more heavily, since the photo-emitted electrons from these layers have a lower probability of inelastic scattering. The sampling depth is ~4–6 nm, and ~10% of the signal originates from the outermost atomic layer. This near-surface region is inhomogeneous because the AO reacts with the outermost few atomic layers. Therefore, the region that is affected to the greatest extent as a result of the reaction

Table 8.1 Near-surface composition determined from XPS data obtained from the as-entered, solvent cleaned, AO, and air-exposed 20-wt% POS-PU sample. Reprinted from [15] with permission from Journal of Adhesion Science and Technology.

Surface Sample Treatment	AO fluence O/cm^2	Composition (at. %)						Atom ratio
		O	Si	C	Sn	Na	N	O/Si
As-entered, solvent cleaned	—	18.5	8.1	72.5	0.9	—	—	2.28
2-h AO exposure	1.44 x 10^17	20.4	7.9	70.7	1.0	—	—	2.58
24-h AO exposure	1.77 x 10^18	21.8	9.5	61.7	1.0	3.0	3.0	2.29
63-h AO exposure	4.53 x 10^18	32.6	11.1	37.8	1.8	13.6	3.1	2.93
4-hr air exposure following 63-h AO exposure	4.53 x 10^18	38.9	13.7	43.4	2.0	2.0	—	2.83

with AO also makes the largest contribution to the XPS signal. This fact implies that XPS is an excellent technique for studying AO erosion of spacecraft materials. Even though both the distribution functions involving the depth of chemical reactions in the near-surface region, and the XPS determination of the weighted average composition of the near-surface region are complex, the compositional values provide a trend which is indicative of the chemical alterations occurring during AO exposure. The compositions determined using the homogeneous assumption are shown in Table 8.1 as a function of AO fluence. The O/Si atomic ratio is 2.28 for the as-entered sample; increases to 2.58, decreases to 2.29 and again increases to 2.93 after the 2, 24, and 63 hour AO exposures respectively. After the 4 hour air exposure, the O/Si atomic ratio is 2.83, but C also accumulates on the surface during the air exposure. The decrease in the O/Si ratio to 2.29 after 24 h of exposure could be attributed to the relative increase of Na and Sn on the surface. However, the overall increase in the O/Si atomic ratio resulting from exposure to the AO flux is a trend that has previously been observed in two other similar studies of a POS–PDMS (polydimethylsiloxane) and 60 wt % POS–PU copolymer.

It is attributed to the formation of SiO_2 and is consistent with the high-resolution spectra that follow. A significant reduction in the C 1s peak is observed as a result of the incremental exposures to the O-atom flux. The near-surface C concentration decreases from 72.5 atom % for the as-entered sample to 37.8 atom % after the 63 hour exposure. This decrease in C is most likely caused by the reaction of C in the near-surface region with O to form CO and/ or CO_2 which desorb. The increase in

C concentration to 43.4 atomic % observed after the air exposure, is most likely due to the adsorption of C-containing molecules from the air. Air exposure has been a contributor to erroneous results in the past. High-resolution XPS C 1s, O 1s and Si 2p obtained from the as-received, solvent-wiped POS-PU surface before and after the 2, 24 and 63 hour AO exposures are shown in spectra (a) to (d) of Fig. 8.3. Spectrum (e) was obtained after the 3.3 hour air exposure following the 63 hour AO exposure. Variations in peak shapes and positions are observed between the unexposed, AO-exposed, and air-exposed surfaces, indicating that the chemical species distribution is altered by exposure to the AO flux and then to air.
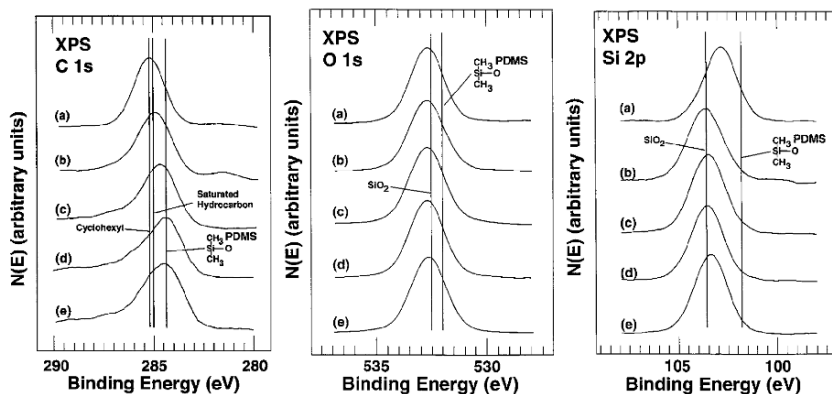
Fig. 8.3 XPS high Resolution C 1s (left), O 1s (center) and Si 2p (right) spectra from a 60 wt % POS-polyurethane (a) after insertion into the vacuum system, (b) after 2 hours, (c) after 24 hours, (d) after 63 hours exposure to the hyperthermal AO flux, and (e) 3.3 hour air exposure following the 63 hour AO exposure. Reprinted from [15] with permission from the Journal of Adhesion Science and Technology.

The C 1s peak, shown in Fig. 8.3 (left), is broad and centered at 285.0 eV, indicating that the predominant form of carbon present for the as-entered POS-PU sample is aliphatic, located on the hard and soft segments of the polymer chain and on the cyclopentyl groups of the POS cages. In spectra (b) to (d), the C 1s peak becomes broader and displays visible shoulders with increasing exposure to the O-atom flux. A shoulder associated with aromatic carbon is present in these spectra at 284.7 eV. Small shoulders are also visible on the high binding energy (BE) side of the C 1s peak in spectra (c) and (d). These are associated with species such as alcohols, formaldehydes (BE -286.0 to 287.7 eV) and organic acids (BE -287.5 eV), which form by reaction with the AO flux. These changes coincide with a decrease in the total carbon concentration in the near surface region, from 70.1 to 37.3 atom %. A dramatic reduction in the carbon concentration after AO exposure was also seen in the POS-PDMS sample studied previously. Exposure to air (spectrum e) produces an 11% increase in C near 285.0 eV, indicating adsorption of hydrocarbons from the air at reactive surface sites produced during the AO exposure. A similar observation was also noted for the POS-PDMS sample.

The O 1s spectra obtained from the as-entered POS-PU sample is shown in Fig. 8.3, center, spectrum (a). This peak is broad and centered at 531.9 eV. The

predominant form of oxygen present for the as-entered sample corresponds to the carbonyl in the urethane segment (531.9 eV) of the polymer and the oxygen present in the POS cages (532.0 eV). Initially, the oxygen contribution is reduced from 18.2 to 17.5 atom % after a 2 hour exposure. Spectrum (b) shows this decrease to coincide with the O 1s peak shifting to a higher BE, and thus decreasing the contributions from the urethane segment and from the oxygen in the POS cages. This reduction is consistent with the production and subsequent desorption of CO_2. After the 24 hour exposure, the near surface O content increases to 23.7 atom %, and the predominant peak featured in spectrum (c) corresponds to silica. This feature becomes more prominent with the 63 hour exposure as the surface O content increases to 35.3 atom %, and is consistent with the formation of an SiO_2 surface. Exposure to air results in a small 3.7 atom % decrease in the surface O content as the reactive surface adsorbs hydrocarbons from the air.

The Si 2p peaks obtained from the POS-PU sample after the various treatments are shown in Figure 8.3 (right). The Si 2p peak for the as-entered sample, spectrum (a), is broad indicating the presence of several chemical states of silicon. This peak is centered at a BE of 102.7 eV, which corresponds to $RSiO_{1.5}$ in the POS cage. However, spectra (b), (c), and (d) reveal the formation of an SiO_2 layer with incremental exposures to the O-atom flux. The fact that little difference is observed in the spectra obtained after the 24 hour and 63 hour exposures indicates that this silica layer forms a protective barrier on the surface which prevents further degradation of the polymer with longer exposure to the O-atom flux. The significant compositional changes observed indicate that most of the near-surface region examined by XPS is altered by the AO exposure.

The chemical reactions that form CO_2 and H_2O are exothermic, so the local surface temperature may be relatively high. This, and the fact that the AO induces a chemically induced driving force, results in diffusion of sub-surface C and H to the surface where they react with the AO. This mechanism is responsible for the subsurface compositional alterations observed using XPS. Again, these findings are consistent with those observed for the POS-PDMS sample.

It was clear from these results that a major focus of the work should be upon making Kapton® polyimide (PI) resistant to AO attack, owing to its extensive use in the space environment. Kapton® polyimide is used widely on spacecraft in flexible substrates for lightweight high-power solar arrays because of its inherent strength, temperature stability, excellent insulation properties, UV stability and IR transparency. It is also used in conjunction with Teflon® FEP (fluorinated ethylene-propylene copolymer) in multilayer blankets for thermal control insulation because of its superior optical properties, including low solar absorbance. In these multilayer insulation blankets aluminum or gold is typically applied to Kapton® owing to these metals' low emissivity.

Over the last twenty-five years, it has been well established through space-based experiments and ground simulations that polymeric materials and films undergo severe degradation as a result of the aggressive environment encountered in LEO [14,17,18]. As noted in the introduction, in this high vacuum environment,

materials are subjected to the full spectrum of solar radiation and must endure constant thermal cycling from -50 ºC to 150 ºC and bombardment by low- and high-energy charged particles, as well as high incident fluxes of AO. These harsh conditions, combined with the need for lighter weight and lower cost man-made orbiting bodies, necessitate the design of space-survivable materials. Thus Tomczak et al. published a major paper in 2005 that addressed this issue with persuasive results [19]. This study expanded the concept of space survivability by the addition of POS entities into the polymer, such that when high energy AO erosion inevitably occurs, the POS materials form a silica passivating layer that prevents further attack and erosion.
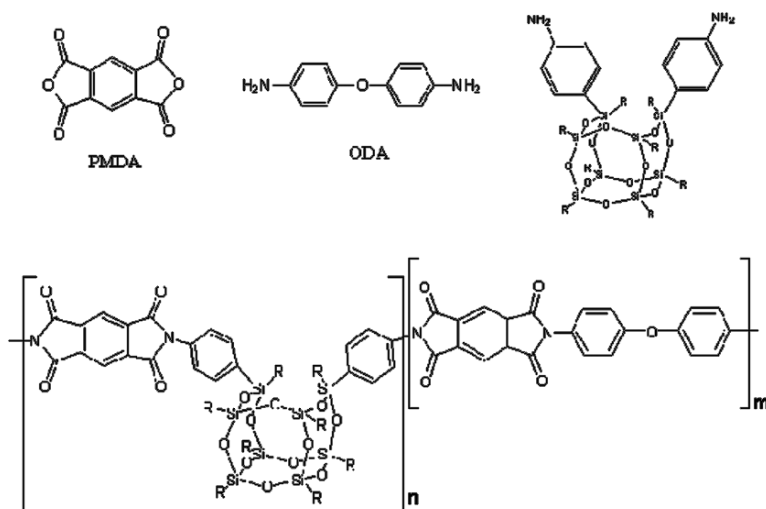
Fig. 8.4 POS Kapton polyimide synthesis. Reprinted from [19] with permission from the Materials Research Society.

Polyimides with the same chemical formula as Kapton® were synthesized via condensation polymerization of 4,4´-oxydianiline (ODA) and pyromellitic dianhydride (PMDA) in an N,N´-dimethylacetamide (DMAc) solvent [20]. A POS framework with two aniline pendant groups was then synthesized [21] as shown in Fig. 8.4. Using this monomer, POS-polyimide random copolymers were synthesized with POS loadings corresponding to 0, 5, 10, 20, and 25 wt %, and were exposed to AO in the pulsed beam hyperthermal facility described above. The mean translational energy of these AO atoms was 4.9 to 5.0 eV, matching the species encountered on orbit. The samples were evaluated before, during and after AO exposure using surface profilometry, atomic force microscopy (AFM) and X-ray photoelectron spectroscopy (XPS).

Fig. 8.5 shows the AFM surface roughness images. It is clear that the increasing concentration of POS in the Kapton® creates substantial resistance to erosion by atomic oxygen. Table 8.2 summarizes the AFM surface roughness data for 0, 10,

and 20 wt % POS polyimide films.
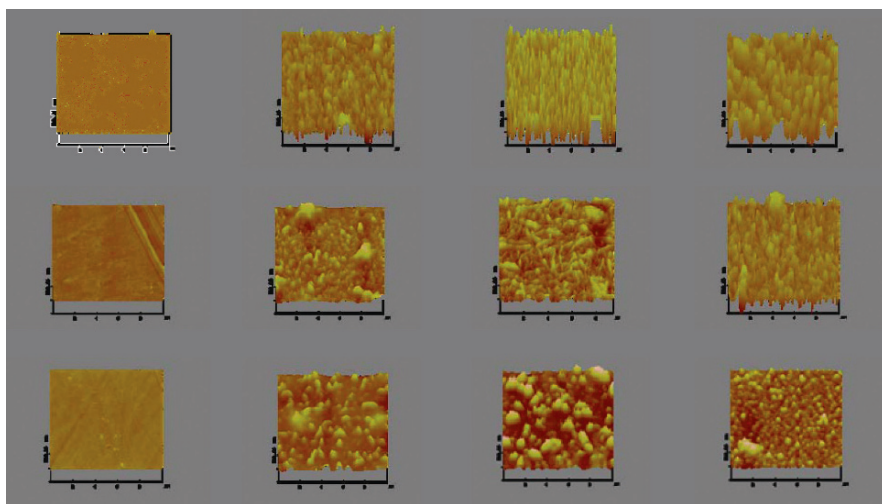
Figure 8.5 Atomic Force Microscopy images of POS polyimides with increasing atomic oxygen flux. (a) 0 wt %, (b) 10 wt % and (c) 20 wt % POS Polyimide surfaces after exposure to atomic oxygen fluences of 0.0, 8×10^{19}, 1.6×10^{20}, and 4.1×10^{20} O atoms cm^{-2}. Reprinted from [19] with permission from the Materials Research Society.

The erosion of Kapton® polyimide is substantially reduced by each successive addition of POS. These erosion rates have been converted into percentages relative to the untreated Kapton®. In addition, a sample of 25 wt % POS-polyimide was exposed to 2.03×10^{20} O atoms cm^{-2}. It showed continued resistance to erosion with this increased POS content. Owing to the very low erosion combined with sample roughness, the step height of erosion of 25 % POS polyimide was not measurable, but was less than the minimum measurable step height of 0.15 µm. The estimated erosion ratio of POS-polyimide to 0 % POS-polyimide for 20 wt % POS -polyimide at 2.03×10^{20} O atoms is 0.046, and that for 25 wt % POS is less than 0.025, showing the erosion decreased by approximately a factor of two with increased POS content. The surface atomic concentrations were measured by XPS, and these results further confirm the mechanisms involved (see Table 8.3).

The hyperthermal AO exposure is provided as the number of pulses from the facility described above. The Kapton® equivalent fluence was determined against a Kapton® H standard. The increasing Si and O concentrations with both POS addition and AO fluence (shown in red) provide solid evidence of the process by which the erosion rate of Kapton® is being reduced by to the formation of a silica-like layer.

A separate exposure of 25 wt % POS-polyimide at a fluence of 7.33×10^{20} O atoms cm^{-2} showed an erosion yield of about 1.1% that of Kapton®. For 0% POS-polyimide, the oxygen concentration approximately doubled, with a greater increase in the POS-polyimides. More importantly, in the POS-polyimides, the silicon concentration reached values of 25%, and at the highest AO fluence the Si:O ratio was approximately 1:2, consistent with the formation of a silica layer.

These surface changes are presumably responsible for the reduced erosion rates

Table 8.2 AFM surface roughness values. Reprinted from [19] with permission from the Materials Research Society.

	AFM RMS roughness values (nm)			
0 wt% POS polyimide	2.48	70	120	126
10 wt% POS polyimide	2.47	22.4	34.3	78.9
20 wt% POS polyimide	2.86	17.2	23.7	39.1
	0	3.8×10^{19}	1.6×10^{20}	4.1×10^{20}

and improved AO reaction efficiencies. Fig. 8.6 shows the effective erosion rates with increasing concentration of POS in polyimide. The fitted curve shows the relationship is exponential with increasing POS content. In the referenced 2005 study, Tomczak et al. explored the use of molecular dynamics simulations to give

Table 8.3 Surface atomic concentrations (%) from XPS scans. Reprinted from [19] with permission from the Materials Research Society.

Sample	AO exposure (beam pulses	Kapton-equivalent atomic oxygen fluence (10^{20} O atoms/cm^2)	C	O	Si	N
0 wt% POS polyimide	0	0	72	19.5	1	7
	6	0.1	69	20	2	9
	100	1.63	69	24	1	6
	250	4.1	55	36	0	9
10 wt% POS polyimide	0	0	77	16	2	5
	6	0.1	73	18.5	5	3.5
	100	1.63	48	30	19	3
	250	4.1	20	56	23.5	0.5
20 wt% POS polyimide	0	0	70	20	6	4
	6	0.1	66	24	7	3
	100	1.63	20	54	25	0
	250	4.1	12	60	26	1

insight into the effect of atomic oxygen on POS-polyimides. They performed molecular dynamics simulations of 5 eV O atom collisions with a POS cage ($Si_8O_{12}H_8$), and with a POS-coated alkane thiol self-assembled monolayer (SAM) on a gold surface. In order to determine the force field for these calculations they used a semi-empirical electronic structure method known as MSINDO (modified symmetrically orthogonalized intermediate neglect of differential overlap). Troya and Schatz had calibrated this approach previously [22] for O atom reactions with hydrocarbon surfaces. In their studies of the reaction of O with the POS cage, they found three reaction pathways: (1) hydrogen abstraction to give OH plus a radical
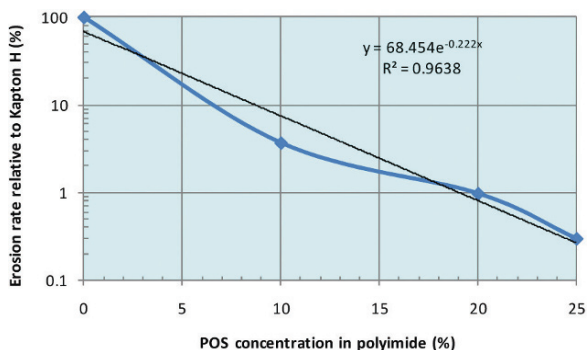
Figure 8.6 Effective erosion rates

cage species (a relatively minor channel), (2) O addition with H elimination to give H plus an oxygenated cage, and (3) O addition with cage opening. Their results show that H elimination and cage opening (by O atom addition to the Si-O bond followed by O-O scission) are the predominant reactions with the POS molecule. Similar mechanisms were found to apply to the POS-coated SAM. These results indicate 5 eV O atoms easily disrupt and oxidize the POS cage. Successive reactions with O atoms would presumably further oxidize the POS, ultimately to give silica.
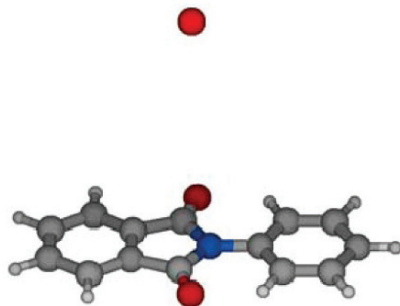
Figure 8.7 QM model of the primary reaction zone. red=oxygen, grey=carbon, blue=nitrogen and white=hydrogen atoms. Reprinted from [19] with permission from the Materials Research Society.

The erosion of polyimide by O atoms involves the breakage and formation of various chemical bonds such as C-C, C-N, C-H, C-O and O-H. Because analytical force fields for O + polyimide were not available, they used a direct dynamics classical trajectory method to simulate the reaction dynamics instead. In the direct dynamics method the classical trajectory is integrated with the forces on each atom obtained directly from quantum mechanical electronic structure calculations (MSINDO semi-empirical calculations in this case). Past studies have suggested that the focus should be upon the electronic ground state potential energy surface, since this makes a dominant contribution to reactivity. A simplified polyimide monomer model (Fig. 8.7) was used for the primary reaction zone and the direct

dynamics calculation was carried out with this model.

Results for a thousand trajectories were generated for 5 eV O atoms colliding with the polyimide monomer is in its ground state with zero point vibrational energy. The unphysical flow of the zero point energy among different vibrational modes (which may cause artificial dynamics behavior especially for systems with large numbers of degrees of freedom) was ignored. Because this simulation was focused on the reactions that occur with the polyimide monomer on a very short time scale (less than 1 ps), the zero point energy flow did not significantly influence the dynamics. The calculations showed that polyimide is very reactive, and over 67% of collisions led to reaction. The classical trajectory simulations revealed a large number of reaction pathways, but O addition reaction was found to be the dominant process. The reaction pathways were grouped into four types: (1) complex formation in which O is added to the monomer without breaking C-C, C-N and C-H bonds (within 1 ps), (2) O addition associated with ring-opening (C-C and C-N bond cleavage); (3) H elimination; (4) OH abstraction. All these reactive channels were found to be exothermic, and hence were thermodynamically allowed. The branching ratios were 1:17:3:3 for reaction types (1) to (4) respectively. Other reaction types were also observed, however they were negligible compared to the above four types of reactions.

Thus in this landmark study it was shown that the incorporation of POS nanostructures into polyimides would likely substantially extend the lifetime of these materials in LEO applications where atomic oxygen erosion is the predominant damage mechanism. Their comparative erosion yields following exposure to a hyperthermal AO source provided clear evidence that POS polyimides exhibited significantly improved oxidation resistance. XPS data and molecular dynamics simulations suggested that this increased resistance was associated with the rapid formation of a self-passivating and self-healing silica layer upon exposure to high fluxes of AO. It was also suggested that this approach could easily be extended to other polymeric systems. Such systems include structural polymers such as polyethylene and polypropylene. Thus this study laid the foundation for a potential revolution in the field of space-survivable materials.

In a subsequent study [23], a series of main-chain POS polyimides (MC-POS-PI) and side-chain POS polyimides (SC-POS-PI) were synthesized with the tailorable side chain organic R-group being cyclopentyl. In this study, there were eight Si atoms, eleven O atoms and eight cyclopentyl groups. This is denoted as Si_8O_{11} because the twelfth oxygen atom has been replaced by two cyclopentyl groups. These materials were exposed to the hyperthermal AO source with results that showed increased AO tolerance with increasing Si_8O_{11} MC-POS-PI additions up to 8.75%. These results demonstrated that POS cages could be incorporated into many different polymeric materials simply by modifying the organic R groups attached to the POS cage.

Table 8.4 CTEs of POS-PI films

Sample	CTE (μm/m°C)
Kapton H®	30.25
0% POS-PI	33.11
7% MC-POS-PI	33.5
8.75% MC-POS-PI	35
7% SC-POS-PI	35.86
7% cage SC-POS-PI	33.64

Finally, because of the sudden temperature changes experienced by materials in the LEO environment, the coefficient of thermal expansion (CTE) is a highly important material property that can impact the usefulness of the POS-PI material. Mismatches in the CTEs between polymeric materials and their coatings lead to cracks, crazing, and mechanical failure. POS-PIs eliminate the need for AO-resistant coatings, but in order for POS-PIs to be a drop-in replacement for Kapton®, it is necessary that the new materials have predictable CTEs with values similar to Kapton®. The CTE values for several samples are shown in Table 8.4. The addition of POS gives a slight increase in the CTE relative to Kapton®. However, a slight decrease is seen after exposure of the SC-POS-PI to AO. The CTE of fused silica is about 0.55 μm m^{-1} °C^{-1}, and the CTE of the silica passivation layer formed on POS-PIs in the presence of AO is expected to be close in value. This mismatch between the silica passivation layer and the underlying POS-PI layer is likely to cause cracks in the silica passivation layer, which will again form silica in the POS-PI exposed areas. Thus this result confirms that the addition of POS to these polymeric materials does not radically change the CTE.

As a confirmatory test, samples of 0, 1.75 and 3.5 wt % Si$_8$O$_{11}$ MC-POS-PI films were exposed to the LEO environment (AO, UV) for 3.9 years as part of the Materials International Space Station Experiment (MISSE-1), and then retrieved and studied. It was found that a 32.55 ± 0.87 μm thick polyimide film was completely eroded. The 1.75 % MC-POS-PI film showed some survival with the inner portion of a circular sample completely eroded and a step height of 5.79 ± 1.31 μm from the outer portion and the masked area, and the 3.5 % MC-POS-PI film maintained a step height of 2.12 ± 0.34 μm from the outer portion and the unexposed area. It was determined by XPS that the atomic percentages of the top 10 nm of the films were 34% Si, 59% O, and 7% C for both the 1.75 and 3.5 wt % Si$_8$O$_{11}$ MC-POS-PI samples. These results confirm the existence of a silica-like layer formation (as also observed in the laboratory tests), and substantiate the model that had been developed.

Thus in this foundational effort, POS addition to a range of polymeric materials was shown to substantially increase their resistance to damage from atomic oxygen in LEO. Mechanical and physical changes of polyimide materials were characterized, and the mechanisms of damage (and of protection) were elucidated. However, the space environment presents two other hazards to spacecraft: UV/VUV light and

particulate radiation (electrons and protons), and the sub-system on a spacecraft that is most affected by both of these hazards is the solar (photovoltaic) array that uses sunlight to produce power for the vehicle.

8.3 Polyhedral Oligomeric Silsesquioxanes in Space Solar Power Systems

A space photovoltaic power array consists of solar cells and their associated cover glasses that are attached together using a clear silicone adhesive. This combination is called a Cover Integrated Cell (CIC). The CICs are interconnected in series into a string of cells that produce the voltage required by the satellite. The strings are placed in parallel to produce the current needed by the spacecraft. The strings of series- and parallel–connected cells are then bonded to a substrate called a face sheet, which may itself be bonded onto an aluminum honeycomb material. This is called a panel. Several panels are connected together and attached to the spacecraft along with a deployment scheme. During launch, the panels are held tightly against the body of the spacecraft and once in space, the panels are deployed, usually on either side of the spacecraft. They are then oriented toward the sun and begin producing power for the vehicle and its energy storage system. Fig. 8.8 shows a typical communications satellite with the solar arrays extended.

Fig. 8.8 Wideband global SATCOM system (U.S. Air Force)

The solar cell cover glasses are fabricated from a special formulation that contains a small percentage of the element cerium. They may also have anti-reflection coatings on the outer surface to maximize the amount of sunlight absorbed. The

cerium addition is very important because it absorbs ultraviolet/vacuum ultraviolet (UV/VUV) light in wavelength bands below about 0.35 μm. This absorption prevents the UV/VUV light from reaching the silicone adhesive, which darkens when exposed to those wavelengths. The cover glasses also protect against the AO in LEO. These cover glasses are very expensive and come in a range of thicknesses (from ~50 μm to 300 μm) to aid in protection against the particulate radiations in space. The thickness of the cover glass is chosen based upon the intended vehicle orbit. For a satellite in GEO, exposed to electrons, protons and solar flare protons, a thickness of 150 μm is sufficient. In LEO the cover glass can be very thin because very little particulate radiation is present there.

Hence because of the costs involved in the materials, as well as the costs from attaching the cover glasses to the solar cells with the silicone adhesive, it was logical to seek an alternative cover glass material that incorporated POS additives, both to provide the protection desired, and to have lower materials and attachment costs. The goal was a highly transparent POS-containing polymeric material that could be deposited by spraying or other low cost application method. It must be resistant to UV/VUV light and proton radiation. Electron radiation is of sufficiently high energy that it generally passes through the CIC. Addressing this would require excessively thick coatings which are not practical owing to high mass.

It was thought that a good first target for the development of this new polymeric cover would be thin film solar cells, because their flexibility may be incompatible with rigid cover glasses. There are several types of thin film solar cells. Some are made of cadmium telluride (CdTe), some of Copper Indium Gallium Selenide (CIGS), and others are made of amorphous silicon. The latter cells were selected for study because they are readily available, are thin and flexible, and are made with a "reel-to-reel" system for low cost. Success with this coating could then extend to other thin film solar cell systems, and could perhaps be transferred to the conventional crystalline GaAs-type multijunction solar cells.

The first use of POS materials was in conjunction with amorphous Si thin film solar cells [24]. The POSS® building blocks used in this study contained hybrid (organic-inorganic) compositions in which the internal frameworks were comprised primarily of inorganic silicon-oxygen bonds. As noted previously, the exterior of the nanostructure is covered by both reactive and non-reactive organic functionalities (–R) that ensure both compatibility and tailorability of the nanostructure with organic polymers. The resulting nanoscopic chemicals have low density, range in diameter from 0.5 to 3 nm, and can be tailored through variation in the R groups and in the size of the nanocage [9,25]. The molecularly dispersed POSS® readily forms a passivating silica layer when attacked by atomic oxygen. This layer in turn protects the virgin material from degradation. Furthermore, the silica-like composition of POS should provide enhanced UV and VUV resistance. The UV and VUV resistance provided by POS can even be enhanced further by replacing for the silicon atoms at the vertices in the nanocage with metals such as cerium. Metal atom addition to the POS nanocages leads to a new designation: polyhedral oligomeric metallic silsesquioxanes (POMS).

In addition, siloxanes (e.g., Dow Corning DC 93-500®, the industry standard cover glass adhesive) are generally considered stable under photo-aging or photo-oxidation conditions. Although they can protect underlying material from oxidation, they do not significantly absorb incident UV radiation, especially if they are alkyl-substituted. A related class of materials that are more highly oxidized and thereby more stable to oxidation and UV are silsesquioxanes. Previous research has shown that chemical manipulation of the organic groups surrounding the POS cage enables dispersion of POS nanostructures throughout the polymer matrix at high POS loadings via blending and co-polymerization techniques described previously.
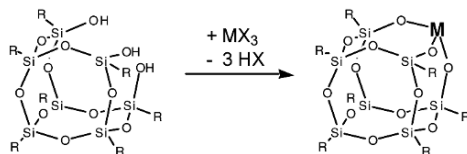
Fig. 8.9 Synthetic method utilized for the manufacture of POMS

For the thin film cell tests, the metalized POS coatings were prepared by adding 10 wt % metalized POS into PM1287 (a siloxane-POS resin). All the metalized POS could be readily dissolved into PM1287 under gentle heat. The incorporation of metals into a POS cage is easily accomplished through the reaction of a POS silanol with a metal halide or alkoxide as shown in Fig. 8.9. A total of five POS coatings: PM1287 control, 10 wt % Ce-POS, 10 wt % Tb-POS, 10 wt % Ti-POS and 10 wt % Gd-POS were tested. Table 8.5 lists the variety of polyhedral oligomeric metallasilsesquioxanes (POMS) prepared, their primary and secondary radiation absorbance targets, and potential component applications. The POMS systems were applied by dissolving them in a high performance conformal coating resin, PM1287. Each of the POMS was found to be soluble at 50-75 wt % levels in the PM1287 resin. Notable advantages of this resin are that it is nonflammable, contains no volatiles, is optically clear, and has a
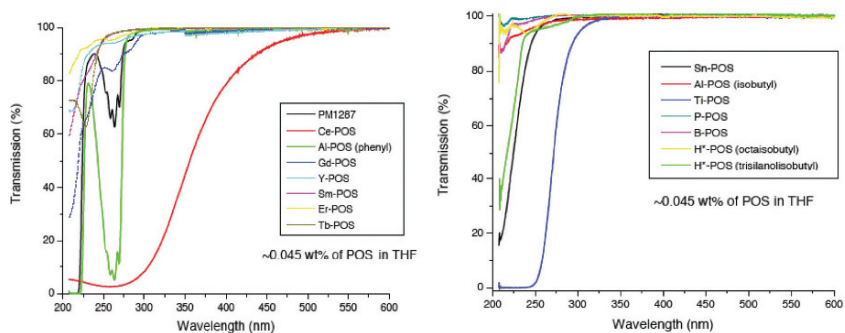
Fig. 8.10 Transmission spectra of various POMS formulations

continuous use temperature of 400 °C. The resin is designed for use as an optically

clear coating, but can also be utilized as a composite resin in both glass and carbon fiber composites. Optical components on space vehicles are known to undergo material degradation, discoloration, loss of optical properties and adhesion due to chain cleavage, and oxidation upon exposure to photonic radiation and X-rays. Such degradation limits the service life and performance level of optical systems. A lower cost solution than deployment of metalized glass cover glasses and vapor-deposited coatings would be to coat sensitive optical components with a polymeric POMS conformal coating that absorbed the damaging incident radiation. The selectivity of POMS toward various wavelengths of VUV through visible radiation is shown in Fig 8.10. The two POMS absorbing the broadest spectrum of radiation are the cerium (Ce) and titanium (Ti) systems. The influence of the R group on the POMS absorption can be seen through examination of the two Al POMS systems.

The Al POMS containing R = Ph is strongly absorptive from 200 to 225 nm, and from 250 to 275 nm, while the Al POMS containing R = *i*-butyl only begins to absorb strongly at 225 nm. Similarly the Gd, Sn POMS also show strong absorptions at 225 nm, while POMS bearing other metals are only weakly absorbing above 200 nm, and absorb strongly below this level. In the light of these properties, the Er, Tb, Al POMS would likely be well suited as protective coatings for radiation below 200 nm. Note that space grade silicone is damaged by 150-160 nm VUV radiation, while polycarbonates are damaged by 243nm UV radiation.

Table 8.5 Radiation targets and applications for various POMS.

POMS additive	Primary targeted radiation	Secondary targeted radiation	Targeted component application
Gd	Neutrons	X-ray, e⁻	ICs
Sm	Neutrons	X-ray, e⁻	ICs
B	Neutrons	X-ray, e⁻	ICs
W	X-ray	e⁻	Sensors, PVs
Ta	X-ray	e⁻	Sensors, PVs
Ti	VUV-UV	X-ray, e⁻	Sensors, PVs
P	VUV-UV	Electrons	Sensors, PVs
Sn	VUV-UV	Electrons	Sensors, PVs
Si	VUV-UV	Electrons	Sensors, PVs
Al	VUV-UV	X-ray, e⁻	Sensors, PVs
H	Protons	e⁻, VUV-UV	IC and Optical
F-	Electrons	Protons	IC and Optical
Ce	VUV-UV	X-ray, e⁻	Sensors, PVs
Tb	VUV-UV	X-ray, e⁻	Sensors, PVs

Each of the POMS systems was found to be suitable for application as a coating on both thin film and triple junction solar cells, since they were optically transparent at 360 nm through longer wavelengths. The adhesion and suitability of Er and Tb POMS in PM1287 as VUV protective conformal coatings for solar

cells was demonstrated by coating a series of active solar cells, and sending them to NASA Glenn Research Center for long term tests which confirmed their stability.

Interestingly, the Tb POMS was identified as being especially beneficial as a solar cell conformal coating, since it was found to absorb short wavelength radiation (200-300 nm) that the cell cannot use, and very efficiently re-emit it through luminescence in the useful 540 nm (green) range. Fig. 8.11 shows a solar cell coated with Tb POMS.
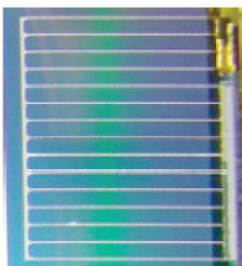
Fig. 8.11 Solar cell coated with Tb POMS

Ten 70 cm² amorphous silicon (α-Si) solar cells were measured before and after coating at the NASA Glenn Research Center under AM0 conditions. Five were coated with the POMS formulations listed above. The coatings were all between 125 and 150 nm in thickness. Fig. 8.12 shows a photograph of the five samples after coating compared to one uncoated sample. This color difference was not unexpected. From left to right the cells are coated with PM1287 control, 10% Ce-POS, 10% Tb-POS, 10% Gd-POS, 10% Ti-POS. An untreated cell is at the far right. From visual inspection, it can be seen that the anti-reflection coating on the cell has not been tailored for the refractive index of the POMS/PM1287, and hence the cells look dark grey rather than black.
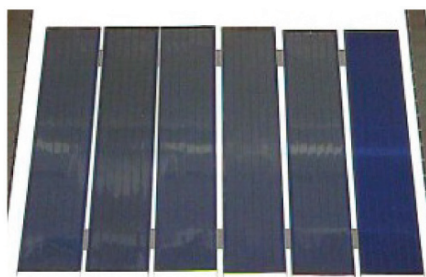
Fig. 8.12 Coated solar cells

Examples of the pre-and post-coating current-voltage (I-V) curves are shown in Fig 8.13. The change in the curve is primarily due to a drop in short circuit current. No significant changes were seen in any of the other components. Table 8.6 provides a listing of the pre- and post-coating cell performance data. The average loss in short circuit current (I_{sc}) for the four cells with the POMS coatings was 6.1%, and the loss in I_{sc} for the PM1287 was 6%. Thus the loss in I_{sc} was the same for all

cells, confirming the mismatch between the refractive index of the POMS (~1.45) and the cell anti-reflection coating. In this test level, no significant change was seen in the open circuit voltage (V_{oc}). Only one cell showed a loss in fill factor (FF), and that was the cell coated with PM 1287 without the POMS additions. Because PM 1287 was used in all the other formulations, this loss, which also impacted this cell's maximum power (P_{max}), is most likely caused by a handling problem, since amorphous Si thin film cells can be easily scratched.
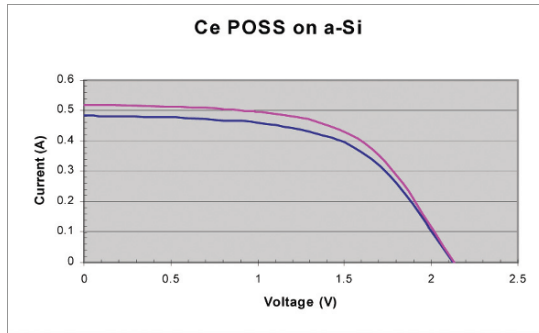
Fig. 8.13 Typical pre- and post-coating I-V curves

Table 8.6 Pre- and post- coating solar cell performance data

Cell coating	Voc (mV)	Isc (mA)	Pmax (mW)	FF (%)	Effic. (%)
Ce POMS pre-	2133	520	647	58.3	6.25
post-	2129	484	591	57.3	6.18
Ce POMS pre-	2143	521	658	58.9	6.87
post-	2131	492	616	58.7	6.43
Ce POMS pre-	2136	517	642	58.1	6.87
post-	2130	485	594	57.4	6.43
Ce POMS pre-	2129	522	652	58.2	6.81
post-	2133	493	613	58.2	6.4
Ce POMS pre-	2140	521	650	58.2	6.79
post-	1964	490	468	48.6	4.88

This was the first test of the application of a PM1287/POMS coating onto thin film solar cells. The coatings were adherent and thermally stable but the optical properties of the anti-reflection coating on the amorphous Si cells was not matched to the refractive index of the coating, hence no further work was done on these samples. It was deemed more important to confirm the radiation stability of these coatings before returning to solar cell applications.

In light of the results on thin film cells, the next steps not only involved looking at the radiation tolerance of the PM 1287, but also developing a new methacrylic POS. For all space applications the materials must be glass-like in their final state, resist AO, UV/VUV and be resistant to electron and proton radiation. Flexibility would be a benefit, but is not essential. In addition, they should be able to be

deposited by spraying or other similar techniques, and, when ultimately applied to solar cells, have excellent adhesion and do not peel away under the extreme thermal cycling conditions that are experienced in space (-100 to +100 ºC). The initial investigation of these new materials was directed toward determining their resistance to low energy proton irradiation. Many space missions are only possible by flying through the heart of the Van Allen radiation belts around the Earth. One mission of this type is a solar electric propulsion mission that moves a satellite from low earth orbit (LEO) to another location. The location may be geosynchronous earth orbit (GEO) as for a communications satellite, or a lunar orbit like ESA's Smart 1. While these missions take more time than using a chemical kick motor, the costs are substantially lower. Other missions of interest are those that would benefit from observing the Earth, and that fly either elliptical orbits that pass through the belts, or that stay within the belts (e.g., the Global Positioning System (GPS) of satellites). The initial study [26,27] looked at the resistance of these coatings to 2 MeV protons. These protons are absorbed in glass-like materials to a depth of about 75 µm, and these coatings were to be about 150 µm thick. Protons are exceptionally damaging to polymeric and other materials because most of the damage occurs at the end of their path, thus causing maximum damage in a very narrow region of the material. If the new materials can withstand this punishment, the next step is generally to assess their resistance to VUV/UV illumination.

Several different compositions of binder and POS additives were used. For most of the samples the binder was either PM1287 as before, or a new methacrylic POS called MA8000. Fig. 8.14 shows the chemical composition of these two binders. The octomeric Si-O cage is the basic building block in PM1287 and is usually introduced via hydrosilylation. To this structure, both metallic additives and organic ligands can be added. In this study, the PM1287 was usually prepared with a phenyl additive in concentrations up to 50%. These additions were generally increased in 10% increments. The MA8000 contained methacrylic additives up to 30%. Several different cure cycles were used from room temperature for long times, to 80 °C cures for a few hours. Metallic additives (POMS) included Gd and B. Both the PM1287 and MA8000 were found to be compatible with the POMS. As described above, the metal is inserted directly into the POS cage and is very stable. The addition of
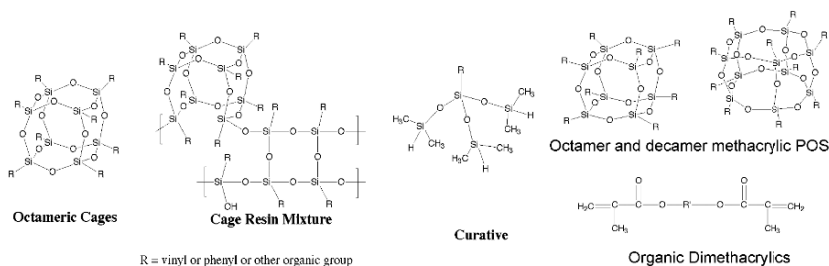
Fig. 8.14 PM1287 structure (left) and MA8000 structure (right)

POMS can further improve the overall performance of those POS based adhesives,

especially if they emit light in the visible region of the spectrum.

The samples were coated onto standard 3.5 cm by 2.5 cm Thales CMG200 Ce-doped microsheet glass slides (the standard solar cell cover glass material). It was used in order to ensure adhesion, and to ensure that the spectral transmission through the layers would be the same as if the coating were used on a solar cell.

PM1287 samples were thermally cured using platinum catalyst. MA8000 samples were cured under UV light. The POS layer was deposited by brush. Optical transmission of the samples was measured between 200 and 1200 nm using an uncoated Ce-doped slide as the background reference. Because an uncoated slide was used as the reference, the data do not take into account transmittance differences associated with reflection at the interfaces.

A 2 MV Dual Source Tandem Accelerator shown is in Figure 8.15. This accelerator can provide a beam of protons from a SNICS ion source with energies from 100 keV to 4 MeV. It can also provide a beam of alpha particles ranging in

Fig. 8.15 NEC Pellatron 2 MV Dual Source Tandem Accelerator

energy from 100 keV to 6 MeV. In addition, a range of heavier atoms including nitrogen, aluminum, and phosphorus can be provided for ion implantation. The ion implantation energies exend up to 12 MeV. For this work, all irradiations were done in vacuum (5×10^{-7} to 1×10^{-6} Torr) and at room temperature. The dose rate was kept constant for each irradiation, with the exception that for the highest dose, the rate was tripled. The initial irradiation was a dose of 10^{12} protons cm^{-2}. After each irradiation the samples were visually inspected for damage , and another transmission spectrum was acquired. The following irradiation total dose schedule was used: second irradiation 10^{13} protons cm^{-2}, third irradiation 10^{14} protons cm^{-2} and fourth irradiation 10^{15} protons cm^{-2}. Beam currents ranged from 55 nA at the lower doses to 190 nA at the highest dose. The proton beam was scanned over a 5 cm diameter area with the samples at room temperature. The scan rate was 517 Hz in the x-direction and 64 Hz in the y-direction. Two samples were irradiated at a time.
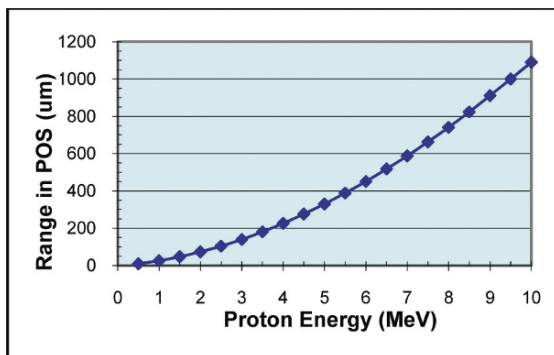
Fig. 8.16 Proton range-energy curve in POS having a density of 1.4 g cm^{-3}
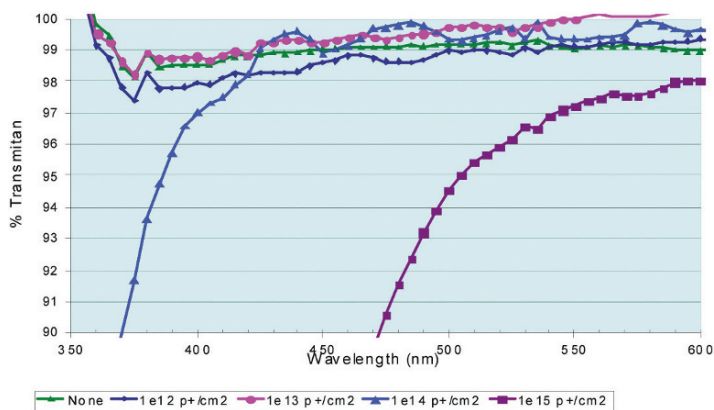
Fig. 8.17 Spectral transmission curves of PM1287 with 50% phenyl content

Fig. 8.18 Images of PM1287 with 50% phenyl content after 2 MeV proton irradiations

The range-energy calculation for the POS materials is shown in Fig. 8.16. These results were obtained using the measured density of the POS materials. At 2 MeV, the range of the protons in POS is 73 μm with a straggle of ~2 μm. Thus the entire proton beam is absorbed within the 150 μm thick POS layer, creating maximum damage within the layer.
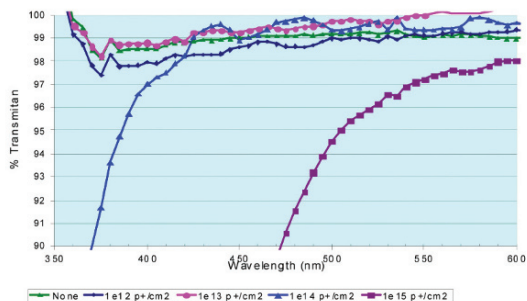
Fig. 8.19 Spectral transmission of PM 1287 with 10% to 50% phenyl content at 10^{12} p+ cm^{-2}
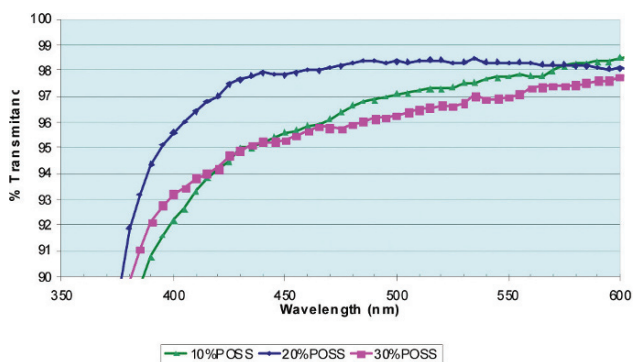
Fig. 8.20 Spectral transmission of MA8000 with various POS additions

Fig. 8.21 Images of MA8000.2 (20% POS) at several proton fluences

The PM1287 resin was tailored to have various possible phenyl contents. The phenyl percentage used herein indicates the mole percentage of the phenyl groups compared to the vinyl groups that are attached to the POS cage (as shown in Fig. 8.14). A total of four samples were made: 10% phenyl, 15% phenyl, 20% phenyl and 50% phenyl. The 50% phenyl PM1287 demonstrated the best proton radiation tolerance as shown in Fig 8.17. The data were limited to the region of interest between 300 and 600 nm. Below 300 nm the CMG200 slide has limited transparency, and above 600 nm the film transmittance does not vary with wavelength. For the sample with 50% phenyl concentration, the transmittance did not decrease until the 10^{14} p$^+$ cm^{-2} dose, and substantial darkening and cracking did not occur until the 10^{15} p$^+$

cm^{-2} dose as shown in Fig. 8.18. For the 10^{12} p$^+$ cm^{-2} dose, the high concentration of phenyl (50%) provided the best radiation tolerance and the lowest concentration (10%) the least tolerance as seen in Fig. 8.19. Because the intermediate 15% and 20% samples do not follow this trend there may be additional factors (i.e. catalyst loading) that affect the radiation tolerance. In addition to darkening, the sample films showed evidence of structural stress at large total dosages. The damage typically started as micro-fractures on the surface which then developed into long cracks, followed by delamination and separation from the cover glass substrate. The 10% and 15% phenyl films cracked during the 10^{13} p$^+$ cm^{-2} irradiation, the 20% cracked 72 hours after the 10^{13} p$^+$ cm^{-2} test, and the 50% phenyl film developed one long crack after 10^{15} p$^+$ cm^{-2}. These results suggested that the thermal expansion coefficient on the PM1287 was larger than the cerium-doped microsheet glass, and the additional shrinkage of the film caused by the proton irradiation was causing ultimate failure of the films.

The same procedures noted above were followed for the MA8000 samples. For MA8000 samples, the amount of functional POS molecules dissolved in the
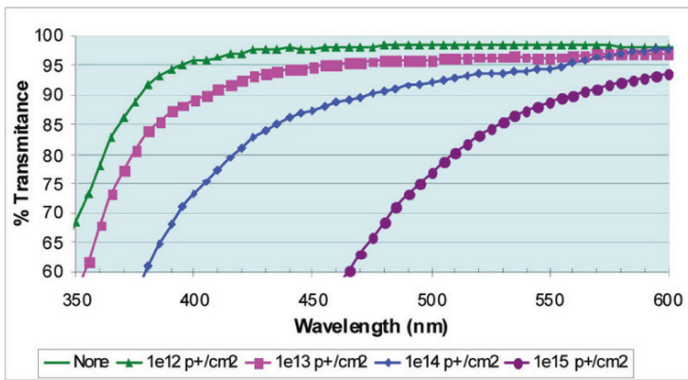
Fig. 8.22 Optical transmission curves of MA8000.2 (20% POS) with increasing proton dose
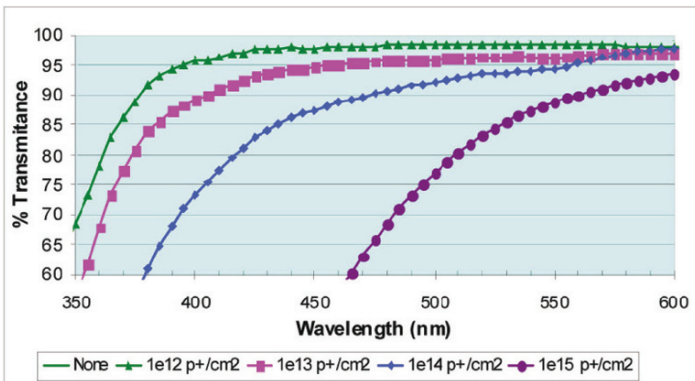
Fig. 8.23 External quantum efficiency of a typical ATJ space solar cell

polymer was directly related to the films' radiation tolerance. Three samples, 10 wt %, 20 wt %, and 30 wt % POS-reinforced MA8000 (MA8000.1, MA8000.2 and MA8000.3, respectively) were made. These samples were more opaque below 500 nm than were the PM1287 samples, as shown in Fig. 8.20. The sample with 20% POS in MA8000 was the most transparent, and showed the least radiation-induced darkening (see Fig. 8.21). Layers based on MA8000 also showed indications of stress within the film after irradiation, just as had been seen with the PM1287 films.

At 10^{14} p$^+$ cm^{-2}, both the 10% and 30% POS samples cracked, but the 20% POS sample did not crack until the 10^{15} p$^+$ cm^{-2} irradiation. Photographs of the MA8000 with 20% POS are shown in Fig 8.21 and the spectral transmission curves are shown in Fig. 8.22 (note the scale change). The darkening of the sample seems very great at the 10^{15} p$^+$ cm^{-2} dose level. Because spectral transmission curves by themselves do not give any indication of the performance of a solar cell beneath that layer, another study was performed to attempt to quantify this loss.
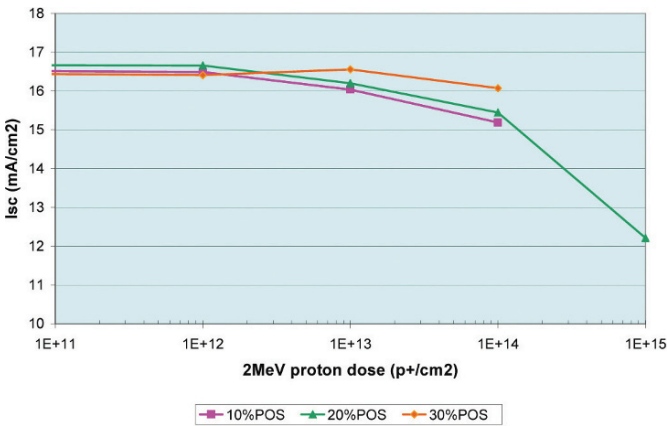
Fig. 8.24 Calculated I$_{sc}$ variation with 2 MeV proton dose for PM1287-coated samples

This is a most informative approach because the internal quantum efficiency of the solar cell determines the ultimate performance beyond any darkening of the cover glass or encapsulant material.

Thus, in order to predict the effect of the observed cover material darkening on the performance of a solar cell assembly, the transmittance of each sample was multiplied by the quantum efficiency of a typical EMCORE Photovoltaics, Inc. ATJ triple junction solar cell, in order to determine the short circuit current, I$_{SC}$. The ATJ quantum efficiency is shown in Fig. 8.23. Because the three junctions are in series, the junction that produces the least current controls the output of the cell. The I$_{SC}$ calculated for this typical ATJ cell is 17.1 mA cm^{-2}. This value agrees well with data provided by the company. As expected, the middle junction (indium-gallium-phosphide, InGaP) controls the short circuit current. The lowest junction captures much more current in the infrared region, but the InGaP junction limits the current.

Because the transmittance measurements were made using an uncoated cover glass for reference, the data do not incorporate the effect of reflective losses at the interfaces. A final solar cell design tailored for the POS encapsulant would include optimization of the anti-reflective coating between the cell and the cover material as noted for the thin film solar cell samples. Fig. 8.24 indicates that the PM1287 with 50% phenyl showed no decrease in I_{SC} for dosages up to 10^{14} p$^+$ cm^{-2}. Even at lower phenyl substitutions, the I_{SC} decrease was less than 5% for the sample containing 10% phenyl with a dose of 10^{13} p$^+$ cm^{-2}. Although the darkening of the MA8000 was more substantial, the decrease in I_{SC} for the 30% POS sample at a 10^{14} p$^+$ cm^{-2} dose is only 2%. This dose is roughly equivalent to the radiation dose received over a 20 year mission in GEO. Thus the stability of this POS coating is quite acceptable for that type of mission. However, it is important to note that there will be additional solar cell degradation that is not taken into account in this study.

The results show that the material compositions exhibit a regular progression in resistance to damage by 2 MeV protons as the phenyl content increases in the PM1287 resin, and as the POS content increases in the MA8000. It is important to note, that with the calculated I_{sc} of an ATJ cell for these coatings, the PM1287 with 50% phenyl substitutions decreased by only about 13% at 10^{15} p$^+$ cm^{-2}. This shows exceptional durability. Furthermore, the MA8000 with 20% POS showed a 17% drop under the same dose. It can be speculated that the chemical stability of the phenyl group may play a key role in limiting proton damage in these tests.
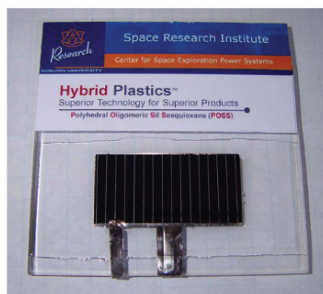
Fig. 8.25 Solar cell with POS conformal coating

While these results were very encouraging, many other space durability tests had to be taken into account. First among these is UV/VUV testing. The cracking seen in the coatings is also a serious concern. Because of the inherent adaptability of the material compositions of the POS, it may be possible to find solutions to the cracking, and ultimately to the darkening of these unique materials. While these coatings must be applied to current production cells to confirm that no inherent damage occurs to them, preliminary work with thin film solar cells uncovered no problems. These coatings are exceptionally clear, and are able to conformally coat solar cells (Fig. 8.25). This is a key factor in the protection of solar arrays from arcing in GEO orbit. The coating should prevent the charge build-up that is a precursor to an arc.

Recent work [28] on POS-silicone compositions was carried out in order to advance the understanding of these new types of flexible lightweight solar cell coatings through space environmental testing. These tests also aimed to provide information on solar cell coatings having the potential to significantly improve mission capability (reduced solar array weight and volume), to increase the solar array lifetime (increased radiation hardness), and to reduce the solar array cost (simplified manufacturing process). POS trisnorbornyl carrying additional *i*-butyl and/or *i*-octyl alkyl groups was used with DC 93-500, resulting in a 20 wt % reinforced DC 93-500® silicone material. Commercial cover glass materials coated with this resin were evaluated for their response to low energy proton radiation simulating the effects of the proton space environment. Exposures for multiple orbits including LEO (833 km, 98° inclination), Global Positioning System (GPS, 20,372 km, 55° inclination) and GEO (35,688 km, 0° inclination) were planned.

Table 8.7 Proton 10 year orbital simulations

Proton energy	Fluence (p$^+$/cm^2)	Fluence (p$^+$/cm^2)	Fluence (p$^+$/cm^2)
Energy (keV)	GEO	GPS	LEO
	10 Year	10 Year	10 Year
400	1.2E+13	1.84E+14	2.29E+11
300	2.74E+13	2.28E+14	1.55E+11
200	1.18E+14	6.19E+14	3.43E+11
100	3.58E+14	1.26E+15	1.00E+12
50	1.03E+15	1.80E+15	1.60E+13
20	2.54E+16	1.08E+16	1.00E+15

Radiation transport modeling was used to generate energy absorption relationships for the following systems: DC 93-500 coated bare Ce-doped cover glass, 20 wt % POS (DC 93-500 – NB1070) coated microscope slide, and an antireflection (AR) coated Ce-doped cover glass. The initial one year GPS orbit proton test was performed on these three systems. The minimum thickness of the POS-silicone coating was 8 μm. Table 8.7 provides the proton energy distributions and doses for 10 years in the three orbits. Optical transmission spectra were measured for all samples, and convolved with a typical triple junction solar cell quantum efficiency, and with the outer space (AM0) spectrum to obtain an estimate of potential current loss for one year in this high radiation orbit. These results, though preliminary and not done at the 10 year level, showed slightly greater loss for the 20 wt % POS (DC 93-500 – NB1070) compared to the DC 93-500 coated slide. Both showed 98.3% current remaining for the solar cell. The AR coated cover glass retained 99.7% of its initial current. These tests show promise for the POS system, but are not conclusive at this time. Much more work on specific compositions must be done to ensure that POS systems are useful for this application. It should be noted that the very low energy protons at 20 keV are exceptionally damaging because they are absorbed in the topmost layer of the material. The 400 keV protons are absorbed within the first

6 μm of the film.

Initial UV/VUV testing was done with four different samples: PM1287 with 50% phenyl content, MA8000.2, PM1287 with Gd POMS, and PM1287 with Tb POMS. The metallic additives were selected to determine if stability of the films was enhanced under these test conditions. The samples were tested for 1024 hours in the UV/VUV testing facility at the NASA Glenn Research Center. The exposures were made in a vacuum chamber using a deuterium lamp (Hamamatsu L7293) that provides radiation as low as 115 nm. The lamp is outside the chamber (to prolong its life) and the radiation is transmitted into the sample through a magnesium fluoride window. The transmission spectra were converted into a calculated J_{sc} loss for an ATJ cell. These results are shown in Fig. 8.26. It appears that the MA8000.2 and the PM1287 with the Tb POMS showed saturation of damage, but this is not conclusive.
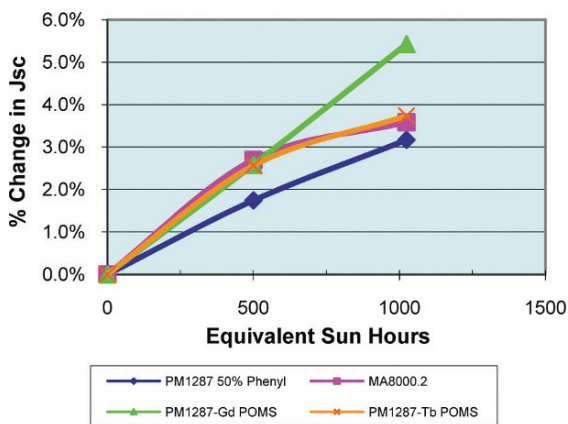
Fig. 8.26 UV/VUV preliminary test results

Interestingly, as noted in Fig. 8.11, the terbium POMS was identified as being especially beneficial as a solar cell conformal coating, since it was found to absorb 'non-useful' 200-300 nm radiation and very efficiently reemit it through luminescence at a 'useful' 540nm wavelength. This green wavelength is absorbed strongly by the top and middle junctions of the triple junction solar cell. As efficiency of the triple junction solar cell increases, the middle junction will play a more important role in radiation resistance and longevity. The application of such a coating would be beneficial, and provide additional photons for energy generation by the solar cell while protecting it against damage by unusable higher energy VUV wavelengths. The high atomic mass of terbium is also beneficial, since it provides shielding against proton, electron, and X-ray radiation. This work is still ongoing.

Because of the potential for a conformal solar cell coating, attention was devoted to producing a sprayable form of a clear, colorless POS-polyimide formulation. The POS-polyimide chain is depicted in Fig 8.27. This new material resulted from a collaborative effort between Hybrid Plastics, Inc. and Mantech International Corporation. This material received an IR100 award in 2008 and is marketed under
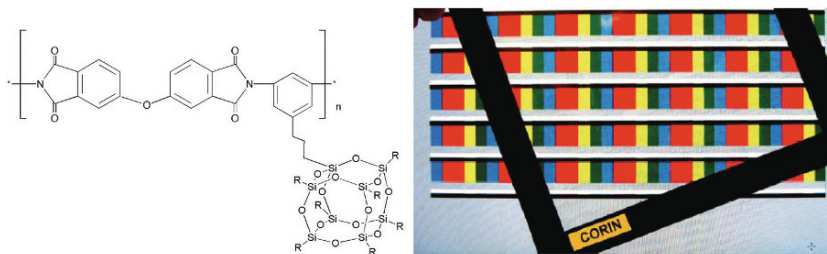
Fig. 8.27 Clear POS-polyimide formulation and its optical properties

the name Corin XLS at Mantech, and POSS® ImiClear at Hybrid. A 25 μm thick film has a 50% transmission cut-off wavelength of 392 nm, making it suitable as a coating for space solar cells. The refractive index is 1.54 and its solar absorptivity is 0.08 at a thickness of 25 μm. Its coefficient of thermal expansion is 68μm m^{-1} °C^{-1}. Although this is much greater than that of a solar cell alone, space solar cells are mounted on various substrates, so the thermal performance of the package can be tailored to the required specification.
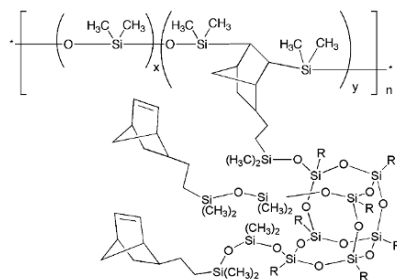
Fig. 8.28 Silicone-tris-norbenyl (isobutyl)$_7$POS network

Because of the need for a compliant POS solar cell covering material, Hybrid Plastics has developed two compliant adhesive POS silicone formulations. The primary difference is the POS loading (20% versus 40%). POSS® Coat SC4300 is a two-part adhesive coating that contains 20% POS loading and POSS® Coat SC4302 contains 40% of the trisnorbornyl(isobutyl)$_7$POS additive (Fig. 8.28). It can be used as an encapsulant, a protective coating or as an adhesive. It is important to note that the silicone used in this formulation is not the industry standard space silicone Dow Corning DC 93-500®. A 20% POS loading into DC 93-500 was demonstrated, and a flight experiment (TacSat-4) has a single multijunction solar cell covered with that material. However, because of the high cost of the space silicone, lower cost silicones are used for POSS® Coat SC4300 and POSS® Coat SC4302. These formulations cost three to six times less than DC 93-500.

The future of these coatings as replacements for cover glasses on solar cells is unclear at this time. It appears that the commercial adoption of a polymeric coating as a general replacement for solar cell cover glasses is unlikely. The reason for

this is that the range of orbital radiation environments is extremely varied, and the need for decades of flight heritage to mitigate mission risk is essential. However, technically, such an effort is achievable. This work has shown that radiation shielding can be achieved using POS polymeric systems. Both radiation-resistant compliant adhesives and radiation-resistant polymer films for glass microsheets have been developed and tested. It appears that the best prospects for deployment of such materials would be on thin film solar cells, if or when they are used in space. While they appear to save mass and volume, their low efficiency requires larger areas that could interfere with the satellite sensors. At present, no similar drivers exist for crystalline solar cell arrays. However, if mission power requirements were to increase greatly, then radiation-resistant conformal coatings for high power arrays would be considered mission critical, since array reliability and mitigation of cell electrical arcing (short circuits) would likely become a critical path. Before any of those uses can occur, the results of space tests such as the MISSE exposure tests must provide persuasive evidence of success.

8.4   Summary

Hybrid inorganic-organic polymers containing POS monomers were synthesized, characterized and tested for atomic oxygen resistance. Samples were placed in a specialized AO source, with the ability to perform in-situ XPS analysis. For both the POS-polydimethylsiloxane and POS-polyurethane systems a passivating SiO_2 layer formed, resulting from the AO-induced degradation of the organic components and subsequent oxidation of the POS framework. Changing the composition of the backbone of the polymer system from entirely inorganic (POS-PDMS) to an inorganic-organic hybrid (POS-PU) does not adversely affect the formation of the SiO_2 layer. Furthermore, the resulting ceramic SiO_2 layer serves to rigidize the elastomeric materials and prevent further degradation of the virgin polymer. These promising results, combined with the numerous property enhancements previously reported for POS incorporation into traditional polymer systems, makes the use of POS an attractive alternative to filler or coating systems in space-based material applications.

    The surface of a film of a POS-PU copolymer was characterized in situ using XPS before and after exposure to different fluences of AO produced by an ESD hyperthermal oxygen atom source. XPS data indicated that exposure to AO reduces the carbon content on the surface from 72.5 to 37.8 atom % after 63 hours exposure to an AO flux of 2.0×10^{13} atom cm^{-2} s^{-1}. The oxygen and silicon concentrations in the near-surface region increase with increasing exposure to the AO flux. The oxygen-to-silicon ratio increases from 2.28 for the as-entered sample to 2.93. High-resolution XPS data suggest that the AO initially attacks the cyclopentyl groups on the POS cage, most likely forming CO and/or CO_2 and water which then desorb.

Increased exposure to the AO flux results in the formation of a silica layer on the surface which acts as a protective barrier, preventing further degradation of the underlying polymer. These results are persuasive in showing that the addition of POS cages to many polymeric systems will enable those systems to resist the effects of AO in LEO, thereby representing a major breakthrough in materials survivability and usefulness in space.

Screening of materials that can be used for an easy-to-apply, space-durable, conformal encapsulant for solar arrays was conducted. The results showed that some of these coatings were exceptionally resistant to damage by 2 MeV protons, which were completely absorbed within the layers. More materials combinations and modifications will be tested over a range of other conditions, beyond proton exposure. Furthermore, the direct application of these coatings onto production solar cells is an essential next step. If this extensive environmental and radiation testing proves successful, a new approach to the total encapsulation of solar arrays will have been demonstrated. With that success, solar array costs should drop, and the development of high voltage arrays for high power space missions should proceed smoothly. However, despite positive results from diligent ground testing, the ultimate verification will only come through successful demonstration in space, owing to the conservative nature of the space business and the costs that failures entail.

We expect that the space market will be transformed by the various POS options, that the impact in performance will be high, and that the reductions in costs will be impressive. Thus the next decade will be exciting to watch!

8.5   References

1.   Banks BA, Demko R (2002) Atomic Oxygen Protection of Materials in Low Earth Orbit, NASA/TM-2002-211360, February 2002.

2.   Banks, BA (1997) The Use of Fluoropolymers in Space Applications. In Scheirs J (Ed) Modern Fluoropolymers: High Performance Polymers for Diverse Applications, John Wiley & Sons, Ltd, Ch. 4.

3.   Banks BA, Rutledge S, Paulsen P, Stueber T, Simulation of Low Earth Orbital Atomic Oxygen Interaction with Materials by Means of an Oxygen Ion Beam, 18th Annual Symposium on Applied Vacuum Science and Technology, Clearwater Beach, Florida, February 6–8, 1989.

4.   Banks BA, Rutledge S, Low Earth Orbital Atomic Oxygen Simulation for Materials Durability Evaluation, 4th European Symposium on Spacecraft Materials in Space Environment, Toulouse, France,

September 6–9, 1988.

5.   Rutledge S, Mihelcic J, The Effect of Atomic Oxygen on Altered and Coated Kapton® Surfaces for Spacecraft Applications in Low Earth Orbit, Proceedings of the Materials Degradation in the Low Earth Orbit Symposium at the 119th annual meeting of the TMS, Anaheim, CA, Feb. 17–22, 1990.

6.   Banks BA, deGroh K, Rutledge S, Haytas C (1999) Consequences of Atomic Oxygen Interaction with Silicone and Silicone Contamination of Surfaces in Low Earth Orbit, NASA/TM-1999-209179, July 1999.

7.   Banks BA, Rutledge S, Sechkar E, Stueber T, Snyder A, Haytas C, Brinker D (2000) Issues and Effects of Atomic Oxygen Interactions with Silicone Contamination on Spacecraft in Low Earth Orbit, NASA/TM-2000-210056, June 2000.

8.   Hung C, Cantrell G, Reaction and Protection of Electrical Wire Insulators in Atomic-Oxygen Environments. NASA TM–106767, AE-8D Wire and Cable Subcommittee Meeting sponsored by the Society of Automotive Engineers, Albuquerque, New Mexico, April 12–14, 1994.

9.   Gilman JW, Schlitzer DS, Lichtenhan JD (1996) J Appl Polym Sci 60:591-596.

10.   Leger JL, Visentine JT, Santos-Mason B, Low Earth Orbit Resistant Siloxane Copolymers, Proceedings of the 18th International SAMPE Technical Conference, October 7-9, 1986, pp. 1015-1026.

11.   Munjal AK, Long Service Life Considerations of Composite Structures for Space Applications, Proceedings of the 23rd International SAMPE Technical Conference, Kiamesha Lake, NY, Oct. 21-24, 1991, Proceedings (A92-51501 21-23). Covina, CA, Society for the Advancement of Material and Process Engineering, 1991, p. 802-816.

12.   Koontz SL, Albyn K, Leger LJ (1991) J Spacecraft Rockets 28:315-323.

13.   Koontz SL, Leger LJ, Albyn K, Cross J (1990) J Spacecraft Rockets 27:346-348.

14.   Koontz SL, Leger LJ, Visentine JT, Hunton DE, Cross JB, Hakes CL (1995) J Spacecraft Rockets 32(3):483-495.

15.   Hoflund, GB, Gonzalez RI, Phillips SH (2001) J Adhesion Sci Technol

15(10):1199-1211.

16.   Hoflund GB, Weaver JF (1994) J Measur Sci Technol (1994) 5(3):
       201-205.

17.   deGroh KK, Banks BA, Techniques for Measuring Low Earth Orbital
       Atomic Oxygen Erosion of Polymers, 2002 Symposium and Exhibition
       sponsored by the Society for the Advancement of Materials and Process
       Engineering, Long Beach, CA May 12-16, 2002.

18.   deGroh KK, Banks BA (1994) J Spacecraft Rockets 31(4):656-664.

19.   Tomczak SJ, Marchant D, Svejda S, Minton TK, Brunsvold AL, Gouzman
       I, Gonzalez RI (2005) Properties and Improved Space Survivability of
       POSS (Polyhedral Oligomeric Silsesquioxane) Polyimides, Material
       Research Society Symposium Proc Vol 851.

20.   Mather PT, Jeon HG, Romo-Uribe A, Haddad TS, Lichtenhan JD (1999)
       Macromolecules 32(4):1194-1203.

21.   Wright ME, Schorzman DA, Feher FJ, Jin RZ (2003) Chem Mater
       15:264-268.

22.   Troya D, Schatz GC (2004) J Chem Phys 120:7696-7707.

23.   Tomczak SJ, Marchant D, Mabry J, Vij V, Minton T, Brunsvold AL,
       Guenthner A, Comparisons of Polyhedral Oligomeric Silsesquioxane
       (POSS) Polyimides as Space-Survivable Materials, 2005 International
       Chemical Congress of Pacific Basin Societies (Pacifichem), Honolulu,
       Hawaii, USA, December 15-20, 2005. (NOTE: this is also available as
       AFRL-ERS-PAS-2006-275. Air Force Research Laboratory (AFMC),
       AFRL/PRS, 5 Pollux Drive, Edwards AFB, CA 93524-7048).

24.   Brandhorst HW, Lichtenhan JD, Fu BX, A POSS® Coating for Thin Film
       Solar Cells, 31st IEEE Photovoltaic Specialists Conference, Orlando,
       Florida, January 2005.

25.   Gonzalez RI, Phillips SH, Holland GB (2000) J Spacecraft Rockets
       37(4):463-467.

26.   Brandhorst HW, Smith TIS, Wells BK, Lichtenhan JD, Fu BX,
       POSS® Coatings as Replacements for Solar Cell Cover Glasses, 19th
       Photovoltaic Research and Technology (SPRAT) Conference, NASA
       Glenn Research Center, Cleveland, OH September 20-22, 2005.

27.   Brandhorst HW, Smith TIS, Wells BK, Lichtenhan JD, Fu BX, POSS®
       Coatings as Replacements for Solar Cell Cover Glasses, 4th World

Conference of Photovoltaic Energy Conversion, May 7-12, 2006, Hawaii.

28.   Liu SH, Granata JE, Meshishnek MJ, Ciofalo MR, Simburger EJ, Space Radiation Environmental Testing on POSS Coated Solar Cell Coverglass, Space Photovoltaic Research and Technology (SPRAT) Conference, Cleveland, OH, 2007.